Chemical Science

ROYAL SOCIETY OF CHEMISTRY

EDGE ARTICLE

View Article Online
View Journal | View Issue

Cite this: *Chem. Sci.*, 2023, **14**, 2928

All publication charges for this article have been paid for by the Royal Society of Chemistry

Received 20th January 2023
Accepted 16th February 2023

DOI: 10.1039/d3sc00355h

rsc.li/chemical-science

Combination of changeable π-conjugation and hydrophilic groups for developing water-soluble small-molecule NIR-II fluorogenic probes†

Xiaofan Zhang,‡[ab] Shili Shen,‡[ac] Diankai Liu,[a] Xiaohua Li,*[a] Wen Shi[a] and Huimin Ma*[ab]

Small-molecule probes emitting in the second near-infrared window (NIR-II) are attracting great attention because of their deep-tissue imaging ability. However, developing NIR-II fluorogenic (off–on) probes with good water solubility remains a great challenge due to the lack of a facile approach. Herein we first report the combination of changeable π-conjugation and hydrophilic groups as an effective strategy for developing water-soluble NIR-II fluorogenic probes. With the strategy, new water-soluble NIR-II fluorophores are prepared, among which NIR-II-F2 and NIR-II-F3 show superior stability and bright fluorescence in aqueous media, and are thus used to design two water-soluble NIR-II fluorogenic probes for leucine aminopeptidase (LAP). The excellent performance in real aqueous bio-environments is demonstrated by imaging mouse vasculatures and organs with NIR-II-F2, and LAP in drug-induced liver injury mice with one of the enzymatic probes; however, water-insoluble dyes cannot achieve such *in vivo* imaging under the same conditions. Our strategy may be helpful for further developing water-soluble organic NIR-II fluorogenic probes for *in vivo* imaging of other analytes.

Introduction

Fluorescence imaging is widely used in the detection of biological species due to its high resolution and sensitivity.[1–3] In particular, the second near-infrared (NIR-II, 900–1700 nm) fluorescence imaging can considerably reduce the light scattering and auto-fluorescence, and thus is more suitable for *in vivo* analysis at deeper penetration.[4–11] There are two main types of NIR-II probes, which are based on inorganic and organic materials, respectively. Inorganic probes have long been accompanied by the controversial toxicity issue, impeding the further clinical application; whereas organic small-molecule probes display the merit of good biosafety as well as flexible structure modification, and have broader prospects for bioimaging.[12–16]

Currently, most of the small-molecule NIR-II probes show a constant always-on signal, thus resulting in a reduced signal-background ratio (SBR). In contrast, fluorogenic (off–on) probes that are responsive to certain stimuli [*e.g.*, pH,[17] H_2S,[18] viscosity,[19] enzymes[20–24] or reactive oxygen species (ROS)[25–29]] give rise to a higher SBR and can achieve accurate and convenient bioanalysis. Generally, there are two common strategies for designing NIR-II fluorogenic probes. They are: (1) incorporation of a recognition moiety into a conjugated NIR-II fluorophore quenches the fluorescence, and then the reaction of the probe with the analyte recovers the NIR-II fluorescence without change of π-conjugation in the system. (2) Design of a changeable π-conjugated system (CCS),[30–32] *i.e.*, the probe itself exists in a less conjugated state and emits no or weak fluorescence; however, its reaction with the analyte leads to the formation of an extended π-conjugated molecule, thereby yielding a strong NIR-II signal. Since the conjugation transformation of the probe is dominantly regulated by the analyte of interest, CCS probes usually display higher selectivity and sensitivity.[33] Unfortunately, such off–on probes in the NIR-II region are rare. Worse still, most of the existing NIR-II fluorophores or probes suffer from poor water solubility, and a high fraction (>10%, v/v) of organic solvents has to be used, which may inevitably cause severe damage to living organisms or give results deviating from real aqueous bio-environments. In fact, water solubility has been a difficult problem in the field of NIR-II probes. Toward this end, liposome encapsulation and PEGylation are frequently employed to improve water solubility.[34–39] However, nanosized agents usually have poor reproducibility, and encapsulation may isolate the direct interaction of the internal probe with the

[a]*Beijing National Laboratory for Molecular Sciences, Key Laboratory of Analytical Chemistry for Living Biosystems, Institute of Chemistry, Chinese Academy of Sciences, Beijing 100049, China. E-mail: lixh@iccas.ac.cn; mahm@iccas.ac.cn*

[b]*University of Chinese Academy of Sciences, Beijing 100049, China*

[c]*School of Chemistry and Pharmaceutical Engineering, Shandong First Medical University & Shandong Academy of Medical Sciences, Tai'an, Shandong, 271016, China*

† Electronic supplementary information (ESI) available: Experimental methods, syntheses and structure characterization, supplementary tables and figures. See DOI: https://doi.org/10.1039/d3sc00355h

‡ These authors contributed equally to this work.

external analyte, thereby decreasing the detection sensitivity. In addition, unlike organic small-molecule probes with a definite molecular weight and structure, nanosized agents are often difficult to accurately characterize and standardize because of their heterogeneity or non-uniformity.[40] On the other hand, direct introduction of hydrophilic groups (*e.g.*, sulfonate and carboxyl) into NIR-II fluorophores also provides an efficient measure to improve water solubility.[3,41–44] For example, introducing two hydrophilic sulfonates enhanced the water solubility of probe FD-1080.[42] Similarly, by the introduction of four sulfonic groups, the resulting NIR-II dyes[43] exhibited obvious fluorescence in aqueous media. Unfortunately, these aforementioned NIR-II dyes can only generate a constant always-on signal, and therefore, they did not show a fluorogenic (off–on) feature. Based on the above analyses, it is obvious that a facile approach to develop water-soluble organic NIR-II probes with a fluorescence off–on feature (*i.e.*, to meet these multiple purposes) is still lacking but quite necessary.

Herein, we first propose the combination of CCS and hydrophilic carboxyl groups as an effective strategy for developing water-soluble NIR-II fluorogenic probes (Schemes 1, S1 and S2; Fig. S13, ESI†). Specifically, two rhodamine fragments are condensed with hydroxyl-containing dialdehydes to form largely conjugated polymethine fluorophores (NIR-II-F1 ∼ NIR-II-F4) with NIR-II fluorescence. In particular, NIR-II-F2 and NIR-II-F3 show superior overall properties in terms of bright fluorescence, good water solubility and stability in aqueous solutions. Moreover, the fluorophores possess the feature of CCS *via* the tautomerization of enol to keto form, and therefore, NIR-II fluorogenic probes can be developed by engineering the enol form with the analyte's recognition moiety. Reaction of the resulting probes with the analyte can remove the recognition moiety, followed by electron rearrangement to generate the more conjugated structure with the recovery of NIR-II fluorescence (Fig. S13†). This feasibility has been demonstrated by using the fluorophores of NIR-II-F2 and NIR-II-F3 to construct two NIR-II fluorogenic probes (Scheme S3†) for leucine aminopeptidase (LAP, a biomarker of hepatic dysfunction[45–48]). Further, one of the enzymatic probes (NIR-II-F2LAP) has been directly employed for *in vivo* imaging of LAP in the model of drug-induced liver injury in aqueous biosystems without encapsulation.

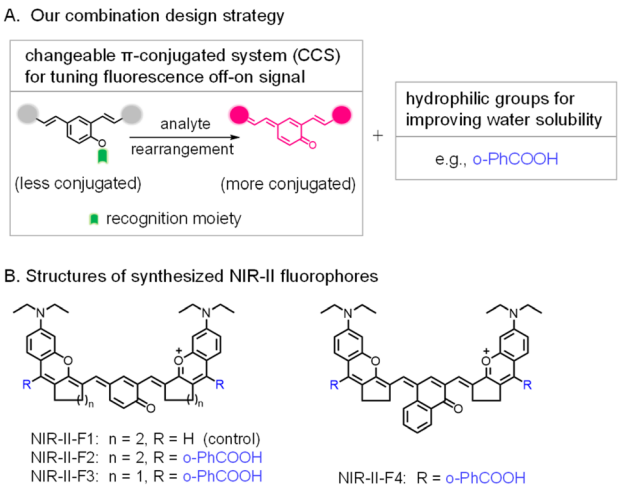

Scheme 1 (A) Combination design strategy for NIR-II fluorogenic probes in this work. (B) Structure optimization of NIR-II fluorophores by introducing functional groups.

Results and discussion

Spectroscopic properties of fluorophores NIR-II-F1–NIR-II-F4

The spectroscopic properties of the fluorophores (NIR-II-F1 ∼ NIR-II-F4) were investigated in various solvents. As shown in Fig. S14,† all the fluorophores exhibit fluorescence emission in the NIR-II region, and the solvent polarity may cause the emission change to varying degrees, among which NIR-II-F4 shows the longest absorption/fluorescence maxima at around 1040/1100 nm in $CHCl_3$. Since good water solubility is usually a prerequisite for application in biosystems, we then studied in detail the photophysical properties of these compounds in phosphate buffered saline (PBS). As shown in Fig. 1A and B and Table S1,† NIR-II-F1 and NIR-II-F2 display similar absorption/fluorescence spectra with different intensities at the maximum peaks (about $\lambda_{abs/em}$ = 590/940 nm). The molar absorptivity (1.9×10^4 $M^{-1}cm^{-1}$) of NIR-II-F2 is about 1.5-fold higher than that (1.3×10^4 $M^{-1}cm^{-1}$) of NIR-II-F1; NIR-II-F2 also shows significant fluorescence (quantum yield Φ = 0.02%; Table S1†), but NIR-II-F1 is nearly non-fluorescent. Moreover, NIR-II-F2 exhibits higher water solubility than the control compound NIR-II-F1 (Table S2†), indicating that the introduction of the hydrophilic *ortho*-PhCOOH greatly improves not only brightness but also water solubility. To explore the

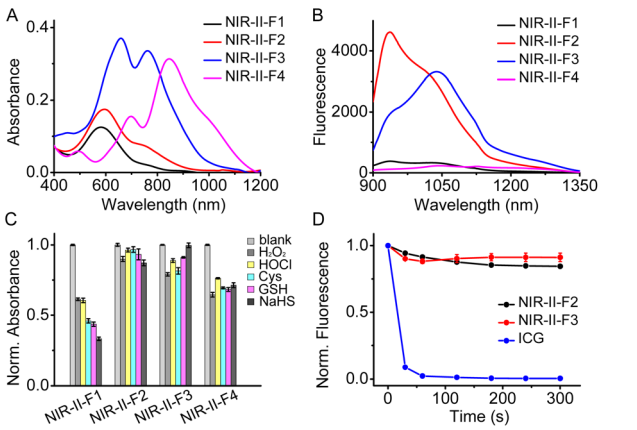

Fig. 1 Spectroscopic characterization of the fluorophores in PBS. (A) Absorption and (B) fluorescence (λ_{ex} = 808 nm) spectra of 10 μM of NIR-II-F1 ∼ NIR-II-F4 in pH 7.4 PBS. (C) Absorbance changes of 10 μM of NIR-II-F1 ∼ NIR-II-F4 in the presence of different redox species: H_2O_2 (10 μM), HOCl (10 μM), Cys (100 μM), GSH (0.5 mM), and NaHS (10 μM). The absorbance of NIR-II-F1 ∼ NIR-II-F4 was measured at 575, 595, 660 and 850 nm, respectively. (D) Photostability of NIR-II-F2, NIR-II-F3 and ICG against an 808 nm laser in pH 7.4 PBS. The fluorescence emission of NIR-II-F2, NIR-II-F3 and ICG was recorded at 933, 1040 and 916 nm, respectively. The results are the mean ± SD (n = 3).

tuning effects of the rhodamine fragments as well as the middle phenol ring on the spectroscopic properties, NIR-II-F3 and NIR-II-F4 were also synthesized. As shown in Fig. S15,† compared to NIR-II-F2, NIR-II-F3 displays significantly bathochromic-shifted absorption/fluorescence wavelengths ($\lambda_{abs/em}$ = 660 760/1040 nm), which may be ascribed to the increased molecular planarity along with the decrease of the saturated carbon number.[49] In addition, as expected, NIR-II-F4 with extended π-conjugation produces larger absorption bathochromic-shifts (λ_{abs} = 700 and 850 nm), compared to NIR-II-F3 (Fig. 1A). Regretfully, although NIR-II-F4 exhibits significant NIR-II fluorescence in organic media such as $CHCl_3$ (Fig. S14†), and its water solubility is as good as that of NIR-II-F3 (Table S2†), NIR-II-F4 emits negligible fluorescence in PBS, which is probably attributed to polaronic quenching of water. Taken together, both NIR-II-F2 and NIR-II-F3 show higher brightness in aqueous PBS, and their emission peaks can even extend to 1300 nm (Fig. 1B and S15†). These data imply that NIR-II-F2 and NIR-II-F3 may have the potential for deep-tissue imaging.

Chemical and photo stability

Due to the presence of various redox species in biosystems, the chemical stability of the fluorophores was examined toward ROS and nucleophiles. As shown in Fig. 1C, the addition of these substances causes a significant absorbance decrease of NIR-II-F1 even by more than 50% in the presence of cysteine (Cys), glutathione (GSH) or NaHS; however, the absorbance of both NIR-II-F2 and NIR-II-F3 changes little (less than 20%), showing superior chemical stability. The improved stability may be attributed to the introduction of *ortho*-PhCOOH, which prevents the oxidative or nucleophilic attack of the redox species on some susceptible chemical bonds. It is noted that the chemical stability of NIR-II-F4 is not so good as that of NIR-II-F3, which might result from the vulnerability of the larger cyanine-like conjugated structure. In addition, NIR-II-F2 and NIR-II-F3 displayed higher photostability than indocyanine green (ICG) under laser illumination (Fig. 1D). The above results suggest that NIR-II-F2 and NIR-II-F3 possess excellent stability in PBS, and may serve as powerful tools for *in vivo* imaging.

Further, pH effects on the fluorescence of NIR-II-F2 and NIR-II-F3 were studied. As depicted in Fig. S16,† the two fluorophores show significant fluorescence under normal physiological pH conditions, and their fluorescence signals at neutral or alkaline pH are stronger than those at acidic pH. The reason for this may be ascribed to the fact that the fluorophores dominantly exist in a more stable keto form with larger conjugation, as illustrated in Scheme S1 and Fig. S13.†

In vivo imaging of mouse vasculature using NIR-II-F2

Because of the higher brightness of NIR-II-F2 than that of NIR-II-F3 (Table S1†), we next applied NIR-II-F2 for *in vivo* imaging experiments. Before that, the half-life time of NIR-II-F2 in mice was determined, being about 34 min (Fig. S17†). NIR-II-F2 exhibited little cytotoxicity (Fig. S18†). Also, the influence of bovine serum albumin (BSA) was tested. As shown in Fig. S19,† the fluorescence of NIR-II-F2 can be largely enhanced after addition of BSA, which may be ascribed to their interaction. The fluorescence enhancement caused by BSA suggests that NIR-II-F2 is suitable for *in vivo* vasculature imaging. Then, we performed such an imaging by injecting the water-soluble NIR-II-F2 into mice without liposome encapsulation; meanwhile, for comparison, both the control NIR-II-F1 and VIX-3 (our previously reported dye)[38] with relatively poor water solubility were injected into mice under the same conditions. As shown in Fig. S20,† bright fluorescence in mice is observed in both ventral and dorsal views for NIR-II-F2; however, the administration of NIR-II-F1 and water-insoluble VIX-3 can hardly light the mice using the same exposure time (ET) and long-pass (LP) emission filter. This clearly demonstrates the outstanding *in vivo* fluorescence properties of water-soluble NIR-II-F2.

The NIR-II images of NIR-II-F2 in mice were also captured using different emission filters. As shown in Fig. 2A, we only observe blurry images, and the body vasculatures cannot be well discerned with a 1000 or 1150 nm LP filter. In contrast, the image resolution can be significantly improved when a longer filter of 1300 nm LP is used. This suggests that although the maximal emission wavelength of NIR-II-F2 is below 1000 nm, the emission peak extending to 1300 nm is useful for high-contrast NIR-II imaging, as well. In addition, clear abdominal (Fig. 2B) and femoral (Fig. S21A†) vessel images can also be

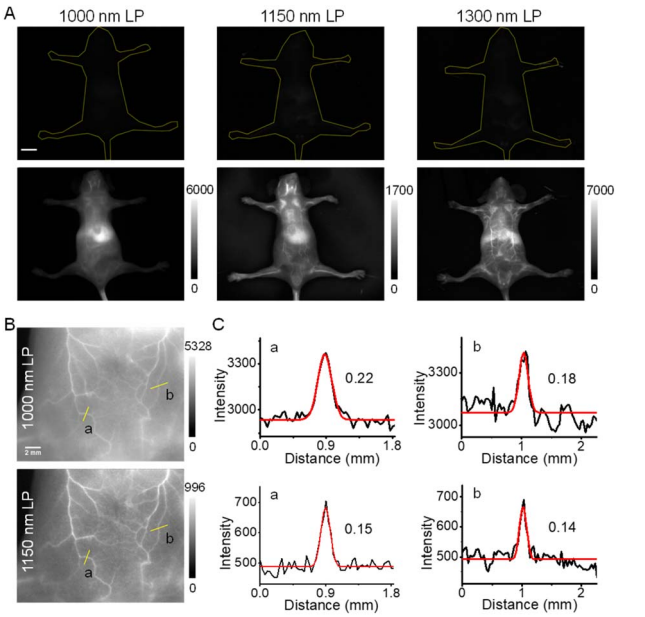

Fig. 2 *In vivo* vasculature imaging with high spatial resolution. (A) Fluorescence images of mice with different filters (1000, 1150 or 1300 nm LP) after injection of NIR-II-F2 (500 μM, 200 μL). Upper row: the images of mice without NIR-II-F2 (control); bottom row: the images of mice with NIR-II-F2. For 1000 nm LP, ET = 10 ms; for 1150 nm LP, ET = 40 ms; for 1300 nm LP, ET = 900 ms. Excitation: 808 nm laser. Scale bar: 1 cm. (B) Abdominal vascular images with a 1000 or 1150 nm LP filter using a higher magnification lens. ET = 250 ms. Excitation: 808 nm laser. Scale bar: 2 mm. (C) Intensity profiles of the corresponding cross-sectional lines (yellow lines labelled with a and b) in panel B with (upper) 1000 or (bottom) 1150 nm LP. The red curve is the Gaussian fitting of the corresponding peak, and the FWHM is marked near the peak.

obtained by using a higher magnification lens even with a 1000 or 1150 nm LP filter; in this case, the use of the longer 1150 nm LP filter is obviously helpful for improving spatial resolution with a smaller FWHM (full width at half-maximum; Fig. 2C and S21B†) and higher SBR (Fig. S21C and S22†). These data reveal the excellent properties of NIR-II-F2 as an NIR-II imaging agent.

Dynamic imaging of blood circulation and organs using NIR-II-F2

Inspired by the high brightness and resolution of NIR-II-F2 in vascular imaging, we further conducted the dynamic imaging of whole-body blood circulation and organs of mice. From the dorsal view (Fig. 3A and Video S1†), the lung lobes were first illuminated within 1.75 s of injection, and then the brain at 2.75 s. After that, a remarkable fluorescence signal was detected in kidneys, followed by the sequential illumination of liver, spleen and back vessels, and the highlighted kidneys were still clearly visible until 20 s of injection. Fig. 3C well shows the illuminating time lag of the organs by the intensity-time analysis. It is known that kidneys are important metabolic organs for water-soluble substances,[50–52] which may explain that NIR-II-F2 with good water solubility can reach and stay in the kidneys without difficulty. Moreover, *ex vivo* biodistribution also confirmed the location of NIR-II-F2 in kidneys (Fig. S23†). It is noteworthy that, although dynamic NIR-II imaging of mouse organs has been performed previously,[11,38] the lighting of all the organs has not yet been achieved. However, based on the sequential imaging with our water-soluble NIR-II-F2, we can clearly observe and distinguish the boundary of lungs, brain, kidneys, liver and spleen.

In addition, dynamic imaging was performed from the ventral view. After injection, NIR-II-F2 lit up heart, lungs, abdominal vessels and liver successively (Fig. 3B and D; Video S2†). Interestingly, when the imaging was made at a higher frame rate of 25 fps (Video S3†), the heart rate was measured to be 320 beats min^{-1} (Fig. S24†), which was higher than our previously reported value (~220 beats min^{-1}).[37,38] A possible explanation may be due to the individual differences or the varied degrees of anesthesia, which can greatly influence the heart rate. It was worth pointing out that the rhythmic fluctuations above the normal intensity were caused by respiration (there were 4 or 5 heart beats between two respirations; Fig. S24B†). The successful measurement of heart rate also demonstrates the capability of NIR-II-F2 for high temporal resolution imaging.

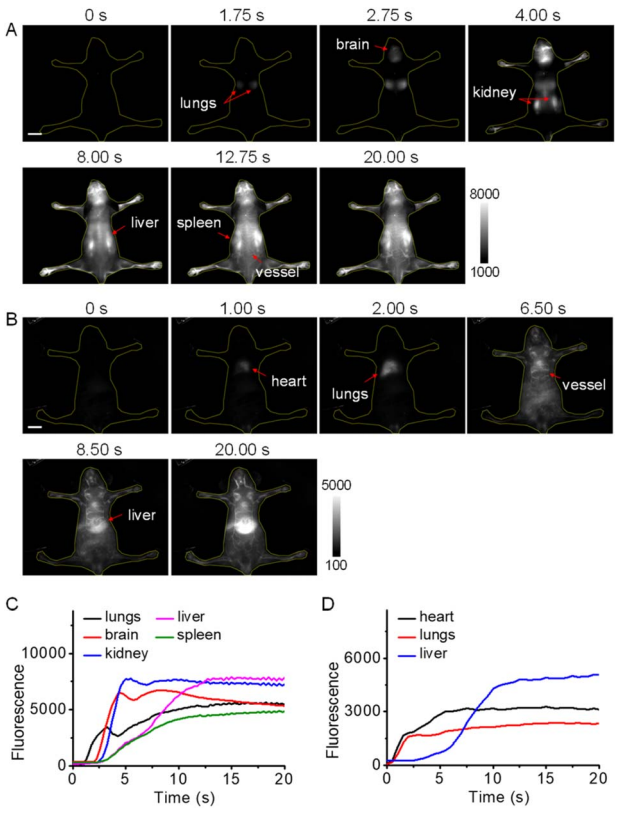

Fig. 3 Dynamic NIR-II imaging of mice with high temporal resolution. Fluorescence images from (A) dorsal and (B) ventral views at representative time points after injection of NIR-II-F2 (500 μM, 200 μL). Excitation: 808 nm laser. For panel A: ET = 250 ms, 1150 nm LP (the corresponding video is shown in Video S1†); for panel B: ET = 500 ms, 1300 nm LP (the corresponding video is shown in Video S2†). The red arrows indicate the illuminated organs at the noted time. Scale bars: 1 cm. (C) Fluorescence intensity of the organs *versus* time in Video S1.† (D) Fluorescence intensity of the organs *versus* time in Video S2.†

In vitro spectroscopic properties of LAP probes

To verify the feasibility of our strategy for developing fluorescence off-on probes, NIR-II-F2 and NIR-II-F3 were further used to design two NIR-II fluorogenic probes (NIR-II-F2LAP and NIR-II-F3LAP) for LAP by introducing the LAP's recognition moiety

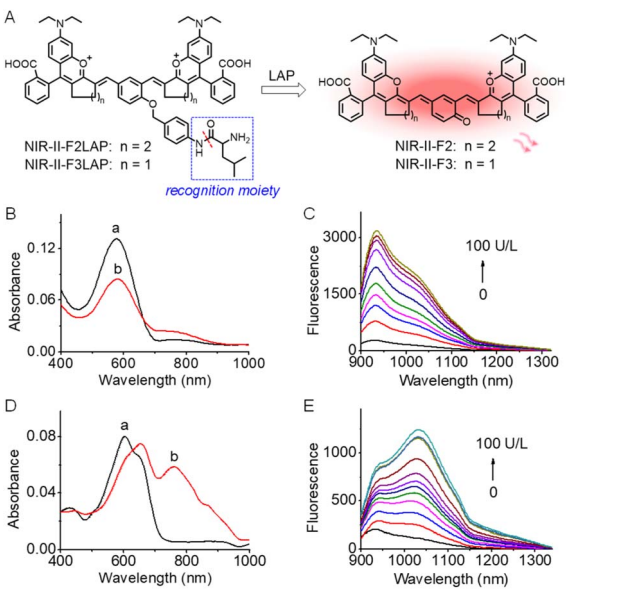

Fig. 4 Structures and spectroscopic properties of LAP probes. (A) Design and sensing mechanism of LAP fluorogenic probes. Absorption spectra of 10 μM of NIR-II-F2LAP (B) and NIR-II-F3LAP (D) in the absence (a) and presence (b) of 50 U L^{-1} LAP in pH 7.4 PBS. Fluorescence spectra of 10 μM of NIR-II-F2LAP (C) and NIR-II-F3LAP (E) with varied LAP (0–100 U L^{-1}) in pH 7.4 PBS. λ_{ex} = 808 nm.

to the hydroxyl of the enol form of the fluorophores (Scheme S3, Fig. 4A and S13†). Due to their good water solubility (Table S2†), the two probes can form homogeneous solution in PBS without liposome encapsulation. Fig. 4B–E show spectroscopic responses of the probes to LAP in PBS. As seen from Fig. 4B, the reaction of NIR-II-F2LAP with LAP leads to the decrease of the absorption peak at 575 nm with a shoulder at 750 nm, concomitant with the emergence of an NIR-II emission peak at 933 nm (Fig. 4C). However, NIR-II-F3LAP reacting with LAP generates bathochromic-shifted absorption peaks from 605/650 to 660/760 nm and an enhanced emission at 1030 nm (Fig. 4D and E). The characteristic spectra of the reaction systems of the two probes coincide well with those of NIR-II-F2 and NIR-II-F3 (Fig. 1A, B and S15†), suggesting the releases of the corresponding fluorophores. High performance liquid chromatography-mass spectrometry analysis (Fig. S25†) clearly proved such a reaction mechanism.

The effects of pH and temperature on the fluorescence responses of the probes to LAP were evaluated. The reactions with LAP proceeded well at pH 7.4 and 37 °C (Fig. S26†), suggesting that NIR-II-F2LAP and NIR-II-F3LAP are suitable for LAP detection under physiological conditions. Moreover, the fluorescence intensity reached a plateau in about 30 min for both probes (Fig. S27†), of which NIR-II-F2LAP showed a faster fluorescence increase. Under the optimized conditions, we next studied the fluorescence changes toward varied LAP. As illustrated in Fig. S28,† the probes exhibit linear increases of the NIR-II fluorescence signal with LAP, and the detection limits (3 S m^{-1}, in which S is the standard deviation of 11 blank solution measurements, and m is the slope of the linear equation) are determined to be 0.063 and 0.188 U L^{-1} LAP for NIR-II-F2LAP and NIR-II-F3LAP, respectively, implying that NIR-II-F2LAP is more sensitive to LAP. The two probes also showed superior selectivity for LAP over various possible coexisting substances in biosystems (Fig. S29†), and inhibition experiments (Fig. S30†) demonstrated that the fluorescence off-on response of the probes indeed arose from the action of LAP.

In vivo imaging of LAP in drug-induced liver injury mice

Finally, we applied NIR-II-F2LAP (with higher sensitivity) to image the change of LAP in the drug-induced liver injury mice, since LAP is identified as a biomarker for the diagnosis of hepatotoxicity. In this experiment, acetaminophen (APAP, a routine analgesic and antipyretic drug) was used to induce liver injury.[47,53–55] Mice were given oral gavage of saline (control) or APAP, followed by the injection of NIR-II-F2LAP; then, time-dependent NIR-II images were recorded. As shown in Fig. 5A, the control group only exhibits weak fluorescence in the liver at 20 min post-injection. In contrast, brighter fluorescence is found in the APAP group, and this fluorescence signal is getting much stronger than that in the control group after 20 min (Fig. 5B). In addition, since viscosity and BSA hardly change the fluorescence of probe NIR-II-F2LAP (Fig. S31 and S32†), the false positive responses from viscosity and BSA are also excluded. These observations suggest a possible upregulation of LAP in APAP-induced liver injury, which was further proved by *ex vivo* biodistribution in the organs (the upregulated LAP mainly from the liver; Fig. 5C and S33†). Moreover, the increased LAP after APAP stimulation was also confirmed by western blot analysis (Fig. 5D). All the above results demonstrated the capability of NIR-II-F2LAP for *in vivo* imaging of the LAP change in drug-induced hepatotoxicity as well as the practicability of our strategy for constructing water-soluble organic NIR-II fluorogenic probes.

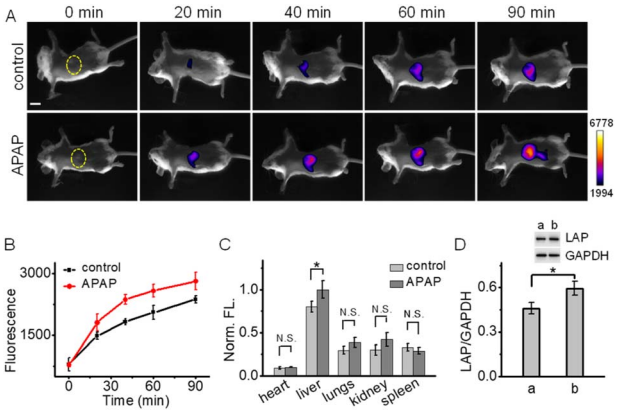

Fig. 5 *In vivo* NIR-II imaging in drug-induced liver injury mice. (A) Representative fluorescence images of mice after receiving oral gavage of saline (control) or 300 mg kg^{-1} APAP, followed by intravenous injection of NIR-II-F2LAP (500 μM, 200 μL). Excitation: 808 nm laser; 1000 nm LP emission filter. Scale bar: 1 cm. (B) Fluorescence intensity in the liver region (yellow circle) from the control or APAP group *versus* time in panel A. (C) Relative fluorescence intensity of the dissected organs at 1 h post-injection of NIR-II-F2LAP. (D) Western blot analysis of LAP in the tissue homogenate of livers from (a) control or (b) APAP group. Glyceraldehyde-3-phosphate dehydrogenase (GAPDH) is used as the protein standard. The results are the mean ± SD (n = 3; each group had three mice). Significant differences (*p < 0.05; N.S. no significant difference) are measured by Student's t-test.

Conclusions

In summary, we have proposed an effective strategy for developing water-soluble small-molecule NIR-II fluorogenic probes, which involves the combination of CCS and hydrophilic groups. With this strategy, we have developed a series of water-soluble NIR-II fluorophores by condensing two rhodamine fragments with hydroxyl-containing dialdehydes. Among them, NIR-II-F2 and NIR-II-F3 show not only excellent chemical and photo stability but also significant NIR-II fluorescence in aqueous media without the aid of liposome encapsulation. Using the water-soluble NIR-II-F2 with higher brightness, high-contrast imaging of vasculatures and organs in mice is successfully achieved, which, however, fails with insoluble dyes under the same conditions. Furthermore, two water-soluble NIR-II fluorogenic probes with high sensitivity and selectivity for LAP are prepared based on NIR-II-F2 and NIR-II-F3. Besides, *in vivo* imaging of the LAP change in drug-induced liver injury mice is demonstrated with one of the enzymatic probes. We anticipate that the proposed combination strategy may be widely adopted for designing water-soluble organic NIR-II CCS probes for other bioactive species.

Data availability

Additional experimental details and data are provided in the ESI. All animal experimental procedures were performed in accordance with the Guide for the Care and Use of Laboratory Animals, and were approved (approval number: SYXK 2017–0033) by Beijing Vital River Laboratory Animal Technology Co., Ltd.

Author contributions

X. Z., S. S. and H. M. were responsible for experimental design and data analysis. X. Z. and S. S. performed the experiments. D. L. and W. S. assisted in mice imaging. X. Z., X. L. and H. M. wrote and revised the manuscript. X. L. and H. M. conceived and supervised the project. All co-authors have given approval to the final version of the manuscript.

Conflicts of interest

There are no conflicts to declare.

Acknowledgements

We acknowledge the financial support from the NSF of China (Nos. 22174147, 22074151, 21922412, 21820102007, and 22174148).

Notes and references

1 X. Li, X. Gao, W. Shi and H. Ma, *Chem. Rev.*, 2014, **114**, 590–659.
2 P. Z. Wang, L. Yu, J. K. Gong, J. H. Xiong, S. Y. Zi, H. Xie, F. Zhang, Z. Q. Mao, Z. H. Liu and J. S. Kim, *Angew. Chem., Int. Ed.*, 2022, **61**, e202206894.
3 H. M. Ma, *Spectroscopic Probes and Sensing Analysis*, Chemical Industry Press, Beijing, 2020.
4 Y. Lai, Y. Dang, F. Li, C. Ding, H. Yu, W. Zhang and Z. Xu, *Adv. Funct. Mater.*, 2022, **32**, 2200016.
5 M. Won, M. L. Li, H. S. Kim, P. Liu, S. Koo, S. Son, J. H. Seo and J. S. Kim, *Coord. Chem. Rev.*, 2021, **426**, 213608.
6 E. D. Cosco, B. A. Arus, A. L. Spearman, T. L. Atallah, I. Lim, O. S. Leland, J. R. Caram, T. S. Bischof, O. T. Bruns and E. M. Sletten, *J. Am. Chem. Soc.*, 2021, **143**, 6836–6846.
7 X. Zhou, K. Zhang, C. Yang, Y. Pei, L. Zhao, X. Kang, Z. Li, F. Li, Y. Qin and L. Wu, *Adv. Funct. Mater.*, 2022, **32**, 2109929.
8 V. G. Bandi, M. P. Luciano, M. Saccomano, N. L. Patel, T. S. Bischof, J. G. P. Lingg, P. T. Tsrunchev, M. N. Nix, B. Ruehle, C. Sanders, L. Riffle, C. M. Robinson, S. Difilippantonio, J. D. Kalen, U. Resch-Genger, J. Ivanic, O. T. Bruns and M. J. Schnermann, *Nat. Methods*, 2022, **19**, 353–358.
9 Y. Lai, Y. Dang, Q. Sun, J. Pan, H. Yu, W. Zhang and Z. Xu, *Chem. Sci.*, 2022, **13**, 12511–12518.
10 F. Sun, W. Zhao, H. Shen, N. Fan, J. Zhang, Q. Liu, C. Xu, J. Luo, M. Zhao, Y. Chen, K. W. K. Lam, X. Yang, R. T. K. Kwok, J. W. Y. Lam, J. Sun, H. Zhang and B. Z. Tang, *Adv. Mater.*, 2022, 2207671.
11 Q. Zhang, P. Yu, Y. Fan, C. Sun, H. He, X. Liu, L. Lu, M. Zhao, H. Zhang and F. Zhang, *Angew. Chem., Int. Ed.*, 2021, **60**, 3967–3973.
12 T. Han, Y. Wang, J. Xu, N. Zhu, L. Bai, X. Liu, B. Sun, C. Yu, Q. Meng, J. Wang, Q. Su, Q. Cai, K. S. Hettie, Y. Zhang, S. Zhu and B. Yang, *Chem. Sci.*, 2022, **13**, 13201–13211.
13 H. Chen, K. Shou, S. Chen, C. Qu, Z. Wang, L. Jiang, M. Zhu, B. Ding, K. Qian, A. Ji, H. Lou, L. Tong, A. Hsu, Y. Wang, D. W. Felsher, Z. Hu, J. Tian and Z. Cheng, *Adv. Mater.*, 2021, **33**, 2006902.
14 T. B. Ren, Z. Y. Wang, Z. Xiang, P. Lu, H. H. Lai, L. Yuan, X. B. Zhang and W. Tan, *Angew. Chem., Int. Ed.*, 2021, **60**, 800–805.
15 Z. Qin, T. B. Ren, H. Zhou, X. Zhang, L. He, Z. Li, X. B. Zhang and L. Yuan, *Angew. Chem., Int. Ed.*, 2022, **61**, e202201541.
16 J. Mu, M. Xiao, Y. Shi, X. Geng, H. Li, Y. Yin and X. Chen, *Angew. Chem., Int. Ed.*, 2022, **61**, e202114722.
17 M. Zhao, J. Wang, Z. Lei, L. Lu, S. Wang, H. Zhang, B. Li and F. Zhang, *Angew. Chem., Int. Ed.*, 2021, **60**, 5091–5095.
18 K. Dou, W. Feng, C. Fan, Y. Cao, Y. Xiang and Z. Liu, *Anal. Chem.*, 2021, **93**, 4006–4014.
19 J. Liu, W. Zhang, C. Zhou, M. Li, X. Wang, W. Zhang, Z. Liu, L. Wu, T. D. James, P. Li and B. Tang, *J. Am. Chem. Soc.*, 2022, **144**, 13586–13599.
20 X. Zhang, X. Li, W. Shi and H. Ma, *Chem. Commun.*, 2021, **57**, 8174–8177.
21 J. Chen, L. Chen, F. Zeng and S. Wu, *Anal. Chem.*, 2022, **94**, 8449–8457.
22 R. Wang, J. Chen, J. Gao, J. A. Chen, G. Xu, T. Zhu, X. Gu, Z. Guo, W. H. Zhu and C. Zhao, *Chem. Sci.*, 2019, **10**, 7222–7227.
23 J. A. Chen, H. Pan, Z. Wang, J. Gao, J. Tan, Z. Ouyang, W. Guo and X. Gu, *Chem. Commun.*, 2020, **56**, 2731–2734.
24 J. Ouyang, L. Sun, Z. Zeng, C. Zeng, F. Zeng and S. Wu, *Angew. Chem., Int. Ed.*, 2020, **59**, 10111–10121.
25 L. Sun, J. Ouyang, F. Zeng and S. Wu, *Biomaterials*, 2022, **283**, 121468.
26 W. Feng, Y. Zhang, Z. Li, S. Zhai, W. Lv and Z. Liu, *Anal. Chem.*, 2019, **91**, 15757–15762.
27 L. Chen, J. Chen, Y. Fang, F. Zeng and S. Wu, *Chem. Commun.*, 2021, **57**, 7842–7845.
28 C. Li, W. Li, H. Liu, Y. Zhang, G. Chen, Z. Li and Q. Wang, *Angew. Chem., Int. Ed.*, 2020, **59**, 247–252.
29 F. Bai, W. Du, X. Liu, L. Su, Z. Li, T. Chen, X. Ge, Q. Li, H. Yang and J. Song, *Anal. Chem.*, 2021, **93**, 15279–15287.
30 W. Shi and H. Ma, *Chem. Commun.*, 2012, **48**, 8732–8744.
31 H. Li, W. Shi, X. Li, Y. Hu, Y. Fang and H. Ma, *J. Am. Chem. Soc.*, 2019, **141**, 18301–18307.
32 H. Zhang, Y. Xu, H. Li, W. Shi, X. Li and H. Ma, *Chem*, 2022, **8**, 287–295.
33 J. Shang, X. Zhang, Z. He, S. Shen, D. Liu, W. Shi and H. Ma, *Angew. Chem., Int. Ed.*, 2022, **61**, e202205043.
34 Q. Yang, Z. Hu, S. Zhu, R. Ma, H. Ma, Z. Ma, H. Wan, T. Zhu, Z. Jiang, W. Liu, L. Jiao, H. Sun, Y. Liang and H. Dai, *J. Am. Chem. Soc.*, 2018, **140**, 1715–1724.

35 H. Ma, C. Liu, Z. Hu, P. Yu, X. Zhu, R. Ma, Z. Sun, C. H. Zhang, H. Sun, S. Zhu and Y. Liang, *Chem. Mater.*, 2020, **32**, 2061–2069.
36 R. Tian, H. Ma, Q. Yang, H. Wan, S. Zhu, S. Chandra, H. Sun, D. O. Kiesewetter, G. Niu, Y. Liang and X. Chen, *Chem. Sci.*, 2019, **10**, 326–332.
37 Y. Fang, J. Shang, D. Liu, W. Shi, X. Li and H. Ma, *J. Am. Chem. Soc.*, 2020, **142**, 15271–15275.
38 D. Liu, Z. He, Y. Zhao, Y. Yang, W. Shi, X. Li and H. Ma, *J. Am. Chem. Soc.*, 2021, **143**, 17136–17143.
39 A. L. Antaris, H. Chen, K. Cheng, Y. Sun, G. Hong, C. Qu, S. Diao, Z. Deng, X. Hu, B. Zhang, X. Zhang, O. K. Yaghi, Z. R. Alamparambil, X. Hong, Z. Cheng and H. Dai, *Nat. Mater.*, 2016, **15**, 235–242.
40 Y. C. Song, J. X. Liu, Y. Y. Zhang, W. Shi and H. M. Ma, *Acta Chim. Sin.*, 2013, **71**, 1607–1610.
41 Z. Lei and F. Zhang, *Angew. Chem., Int. Ed.*, 2021, **60**, 16294–16308.
42 B. Li, L. Lu, M. Zhao, Z. Lei and F. Zhang, *Angew. Chem., Int. Ed.*, 2018, **57**, 7483–7487.
43 B. Li, M. Zhao, L. Feng, C. Dou, S. Ding, G. Zhou, L. Lu, H. Zhang, F. Chen, X. Li, G. Li, S. Zhao, C. Jiang, Y. Wang, D. Zhao, Y. Cheng and F. Zhang, *Nat. Commun.*, 2020, **11**, 3102.
44 A. L. Antaris, H. Chen, S. Diao, Z. Ma, Z. Zhang, S. Zhu, J. Wang, A. X. Lozano, Q. Fan, L. Chew, M. Zhu, K. Cheng, X. Hong, H. Dai and Z. Cheng, *Nat. Commun.*, 2017, **8**, 15269.
45 B. Wang, Z. Chen, X. Cen, Y. Liang, L. Tan, E. Liang, L. Zheng, Y. Zheng, Z. Zhan and K. Cheng, *Chem. Sci.*, 2022, **13**, 2324–2330.
46 H. Li, D. Kim, Q. Yao, H. Ge, J. Chung, J. Fan, J. Wang, X. Peng and J. Yoon, *Angew. Chem., Int. Ed.*, 2021, **60**, 17268–17289.
47 X. He, L. Li, Y. Fang, W. Shi, X. Li and H. Ma, *Chem. Sci.*, 2017, **8**, 3479–3483.
48 Y. Zhang, X. Chen, Q. Yuan, Y. Bian, M. Li, Y. Wang, X. Gao and D. Su, *Chem. Sci.*, 2021, **12**, 14855–14862.
49 Y. Wei, D. Cheng, T. Ren, Y. Li, Z. Zeng and L. Yuan, *Anal. Chem.*, 2016, **88**, 1842–1849.
50 J. Huang, J. Huang, P. Cheng, Y. Jiang and K. Pu, *Adv. Funct. Mater.*, 2020, **30**, 2003628.
51 J. Ouyang, L. Sun, F. Zeng and S. Wu, *Analyst*, 2022, **147**, 410–416.
52 J. Weng, Y. Wang, Y. Zhang and D. Ye, *J. Am. Chem. Soc.*, 2021, **143**, 18294–18304.
53 M. Chen, C. Wang, Z. Ding, H. Wang, Y. Wang and Z. Liu, *ACS Cent. Sci.*, 2022, **8**, 837–844.
54 X. Fan, T. Ren, W. Yang, X. Zhang and L. Yuan, *Chem. Commun.*, 2021, **57**, 8644–8647.
55 Y. Z. Deng and G. Q. Feng, *Anal. Chem.*, 2020, **92**, 14667–14675.